3. An Investigation of the deformation of underground excavations in salt and potash mines

University of missouri-Rolla, 권상기 박사

An Investigation of the deformation of underground excavations in slat and potash mines

Sangki Kwon
Department of Mining Engineering, University of Missouri-Rolla

ABSTRACT : The most widely accepted method for understanding the deformation mechanism of rock is from the use of computer simulation. However, if the changes in rock properties after excavation are significant this will prevent the computer simulation from predicting the deformation with acceptable accuracy. If the deformations are, however, carefully measured in situ, the resulting data can be more useful for predicting the deformational behavior of underground openings, since the effect of the parameters which influence the deformational behavior are included in the measurement. In this study, extensive data analyses were carried out using the deformation measurements from the Waste Isolation Pilot Plant (WIPP), which is a permanent nuclear waste repository. The results from computer simulations were compared with field measurements to evaluate the assumptions used in the computer simulations. For better description of the deformational behavior around underground excavations, several techniques were developed, namely: (a) the calculation of the zero strain boundary; (b) the evaluation of the influence of adjacent excavations on the deformational behavior of pre-excavated openings; (c) the description of the deformational behavior using in situ measurements; (d) the calculation of the shear stress distribution; and (e) the application of a Neural Network for the prediction of opening deformation.

1. INTRODUCTION

Natural salt deposits are considered as the desirable host rocks for permanent disposal of nuclear waste material because of such unique properties as low permeability, high heat conductivity, and ductility. The deformational behavior of underground openings excavated in rock salt is complex due to its strong dependency on stress, temperature, humidity, and time, as well as on many other parameters. Because of this complexity, the prediction of deformation using a computer simulation before excavation usually yields far different results from the actual measurements. Inaccurate prediction by computer simulation is due to the limitations inherent in computer simulations. For instance, prediction by a computer simulation can be accurate only when the stress conditions and material properties of the rock mass before and after the excavation are clearly known. However, it is difficult to describe the time-dependent property change in the rock mass around an excavation.

The weaknesses of computer simulation can be compensated for with field measurements, when a reliable amount of in situ deformation data is collected and interpreted carefully. With systematic analyses of in situ measurements, the influence of parameters such as time, temperature, and opening geometry on the opening deformation can be evaluated. The information derived from actual measurements can also be applied more or less directly to other conditions, while computer simulations and laboratory tests require many assumptions before applying these results to mining design. Thus, there is a great advantage in

using in situ measurements to understand the actual deformation mechanism and in predicting the deformational behavior of underground excavations. Therefore, in situ measurements should be considered as the main information source for understanding the deformation mechanism of underground excavations in rock salt and more research should be carried out to develop techniques which can effectively utilize in situ measurements. However, no recognizable work in developing techniques which incorporate field measurements which can be used for different purposes has been reported to date.

It also should be kept in mind that field measurements cannot easily derive some deformation mechanisms such as the stress distribution and deformational behavior of the rock far from the opening. Because of this, it is necessary to use computer simulation and field data analysis concurrently in order to maximize the capability of computer simulation and field measurements. It is desirable to calibrate the assumptions made, including those of rock properties and in situ stresses, by comparing the results from computer simulation with field measurements. This process is usually called back-calculation. Back-calculation of rock properties from in situ measurements in salt and potash mines, however, is rather difficult, because of the complex time-dependent deformational behavior of the rock. Without back-calculation and without calibration of the parameters assumed in computer simulation, an accurate description of the actual deformation mechanism of an excavation located in rock salt is impossible. Thus, it is highly recommended that techniques be developed, which can describe the exact distribution of stress and strain around an excavation by using in situ measurements. These techniques will be useful, since the influence of the property changes after excavation, and the influence of the changing stresses are already reflected in the measurements and it is not necessary to further consider this influence in describing the actual deformational behavior.

Prediction of the deformation of a newly designed opening is complex due to the time-dependent deformation mechanism of rock salt as well as the large number of parameters which can influence the deformational behavior. Further, the relationships are not constant for different depths, elapsed times, and excavation methods. Computer simulation and regression analysis are the most widely used methods for predicting the deformational behavior of a newly designed excavation. However, the prediction by computer simulation has some limitations as discussed earlier. Prediction based on regression analysis using field measurements becomes progressively more difficult as the number of parameters involved increases. In order to overcome the problems of computer simulation and regression analysis, Neural Network can be used as an alternative tool, since it has outstanding advantages for multi-parametric data analysis.

2. GENERAL DESCRIPTION OF THE WIPP SITE

The Waste Isolation Pilot Plant (WIPP) is a research and development facility authorized to demonstrate the disposal of radioactive waste. The WIPP project began construction of a facility in Carlsbad, New Mexico under the direction of U.S. Department of Energy (DOE) in 1981. The underground facility at the WIPP is located 650 m below surface in bedded salt.

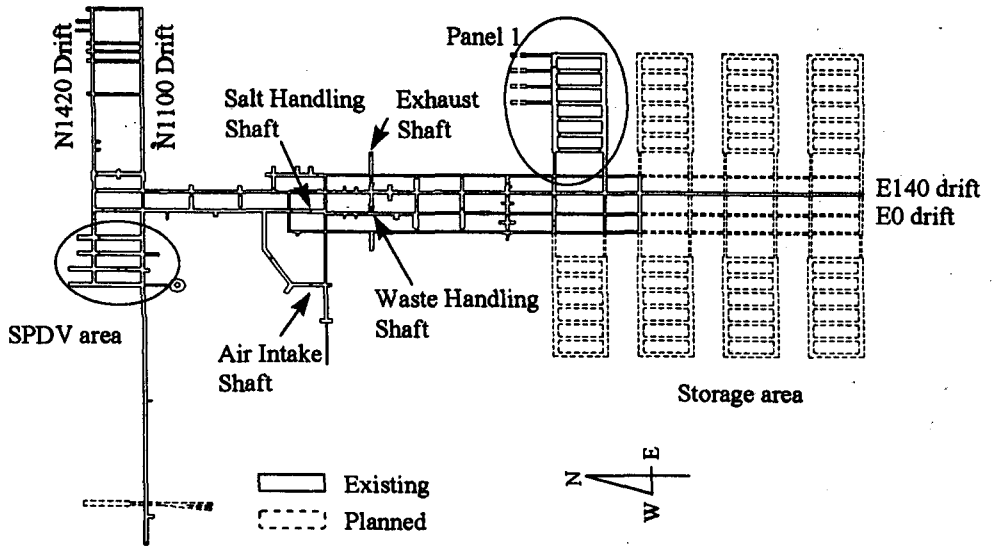

Figure 1 . WIPP underground facility.

The WIPP facility is composed of surface buildings, vertical shafts, and a series of horizontal underground storage rooms, alcoves, and tunnels The underground site has been divided into three areas of the Site and Preliminary Design Validation (SPDV) area, the experimental area, and the waste storage area. The waste storage area will be made up of eight panels consisting of seven rooms each, where each room is approximately 4 m high, 10 m wide and 100 m long. Figure 1 shows the layout of the underground facilities at the WIPP site.

The WIPP facility is composed of four vertical shafts connected to a single underground facility level and the Salt Handling Shaft provides the principal means of access. The Air Intake Shaft serves as the primary air intake opening, whereas the Waste Shaft is designed to permit the transportation of radioactive waste between the surface waste-handling facilities and the underground storage area. The Exhaust Shaft is used for exhaust air from the underground facility.

3. DATA ANALYSIS

Careful investigation of field measurements will identify the influence of each parameter such as opening geometry, in situ stress, temperature, rock properties, geology, and extraction ratio on the deformational behavior of the opening. Data reduction of in situ measurements is critical to derive deformation characteristics related to the governing parameters, because the basic measured data cannot usually be used directly. Any errors in the data should be corrected before data analysis. After this, the data should be plotted appropriately to allow a better interpretation of the deformational behavior.

Various systems of measurement can be used to monitor the performance of underground excavations. Among them, the measurement of closure, which represents cumulative reduction of opening dimensions, is the most general method. At WIPP, several other instruments were used to obtain detailed information on deformational behavior within the rock. The most important instrument is the multi-position borehole extensometer (MPBX) which measures

the relative displacement between the multiple anchors located at various depths in the hole. At WIPP, up to 5 anchor stations were installed in one borehole and most of the extensometers had the deepest anchor placed 15 m from the opening. Another important instrument is the inclinometer. The inclinometer can provide information on rock displacements in a direction perpendicular to the longitudinal axis of the borehole. In the SPDV Rooms, inclinometer measurements have been taken in vertical boreholes up to 15 m deep into the roof and floor (U.S.DOE, 1989).

The field measurements often contain erroneous data because of various reasons. Furthermore, the measurement may not represent the actual deformational behavior of the opening because of other reasons such as anchor slippage or large relative horizontal movement of the layers in the roof or floor.

Extension and closure measurements from the WIPP site were used for general data analysis by well-known analytical techniques such as smoothing, curve fitting, and interpolation. The graphs in Table 1 could be plotted from deformation measurements after running the program.

Table 1. Plotted graphs

1 2 **When the X-axis is cumulative days since excavation** Extension relative to the farthest anchor from the opening Bay extension between the two closest anchors Bay strain between the two closest anchors Total strain between the collar and the last anchor Extension rate Bay strain rate Closure Closure rate Strain acceleration **When the X-axis is distance from the opening** Bay strain Bay strain rate Bay extension Bay extension rate Deflection from an inclinometer Deflection rate

3.1 Influence of opening geometry.

From all available roof extensometers at the WIPP site, the constant extension rates in the steady state creep stage are plotted in Figure 2. There is a relationship between the opening width and the secondary extension rate. With wider openings, the secondary creep rate is higher in most cases. The fairly wide variation in the extension rates might be due to the influence of other controlling parameters such as opening height and pillar size. In most cases, except GE228 at the salt handling shaft, the extension rates of the first 15 m in the roof are below 4 cm/year.

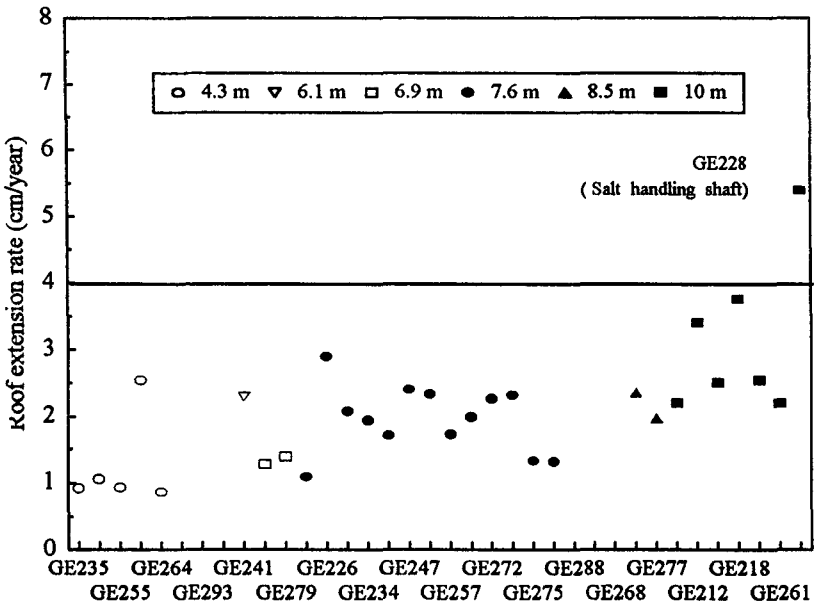

Figure 2. Influence of opening width on the secondary roof extension rate (0.3 m - 15 m).

3.2 Temperature effect.

It is well known that rock salt shows highly temperature-dependent behavior. At higher temperatures, the deformation of rock salt increases due to the plastic flow promoted by the increase in ductility (Hansen et al., 1981; and Wittaker et al., 1992). The measured deformations at the WIPP site shows that the deformations of excavations are affected by the seasonal temperature variation, which varies by about 16 °C. As a result of this study, the following equation is suggested in order to fit the deformation rate curves influenced by seasonal temperature variation, and then to investigate the effect of temperature on the deformation of underground excavations.

$$\dot{\varepsilon} = \left\{A + B\cos\left(\frac{2\pi}{360}\right)\right\}\left\{e^{-\frac{Ct}{365}}\right\} + \left\{D + E\exp\left(-\frac{t}{F}\right)\right\} \quad (3.1)$$

where A, B, C, D, E and F are constants and t is the elapsed days since excavation.

The first part of the above equation is necessary to express the periodic variation. The constant A moves the curve up or down and B determines the amplitude of deformation rate variation due to seasonal temperature change. The second exponential part was introduced to represent the decay of the temperature effect with elapsed time. Depending on the constant C obtained from the best fitting equation, the decay rate of the temperature effect on the deformation rate of the opening can be estimated. A higher C value indicates a more rapid decay of temperature effect with time. The last part defines the general decay pattern of the strain rate when there is no variation related to temperature change. Figure 3 shows the measured data and best fit curve for an extensometer in E0 drift using the above equation.

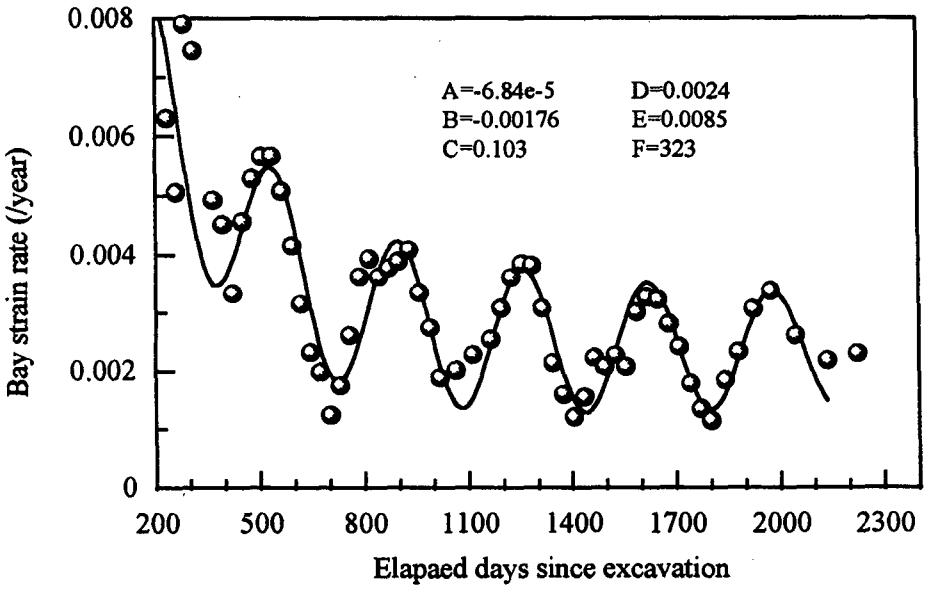

Figure 3. Influence of seasonal temperature variation on deformation rate of 1 m-7.6 m.

3.3 Time effect.

Determination of the transition time from the primary creep stage to the secondary creep stage is essential to define the deformational behavior of the opening. If the transition time is adequately known, it is possible to predict the overall deformation with reasonable accuracy by extrapolating the creep rate of the secondary creep stage, which is a constant.

One possible way to determine the transition zone is to plot all strain rates on a single graph. A Box-Whisker plot is useful for this, since it can effectively describe the mean and distribution of several sets of data in one graph (Verdeman, 1993). In the Box-Whisker plot, the edge of the box enclose the middle 80 % of the distribution, while the "whiskers" define the outlying 5 % of the data values. Figure 4 is the Box-Whisker plot of the first 15 m strain rates in the roof of the excavations at WIPP. The secondary strain rates in the plot were calculated from the linear part of the extension curves. The distribution of the roof strain rates at 200 days after excavation is almost the same as that at 300 days as well as during the secondary creep stage.

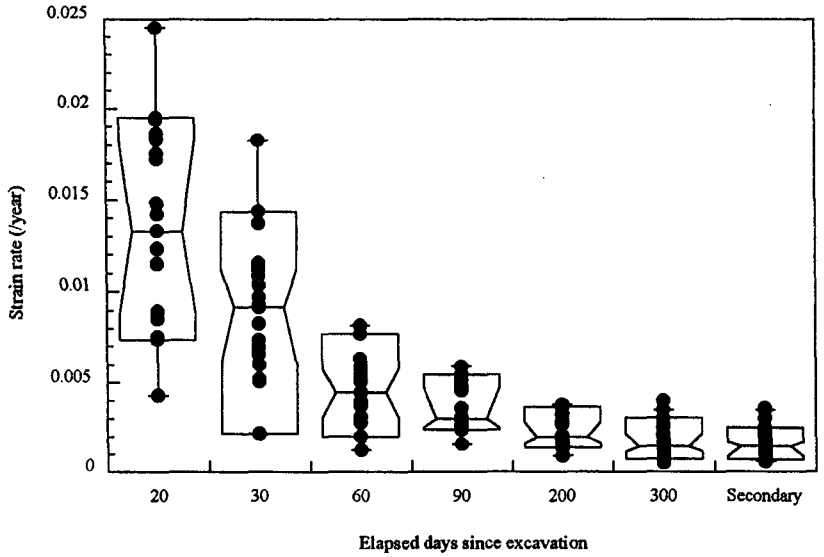

Figure 4. Box-Whisker plot of roof strain rate (0.3 m - 15 m) at WIPP.

3.4 Prediction of a roof fall in SPDV Room 2.

SPDV Room 1 failed on February 4, 1991 about 8 years after excavation. The vertical closure of SPDV Room 1 had been measured until immediately before the collapse. Using these vertical closure measurements, a roof fall in SPDV Room 2 was accurately predicted about 1 year before it happened.

Since the two openings were in almost the same condition, it could be assumed that the roof in SPDV Room 2 would behave in a similar way to that in SPDV Room 1. The closure rate was used for prediction, since it is independent of the time following installation. From the SPDV Room 1 closure rate plot, 20 cm/year (8 in/year) was considered as the critical closure rate preceding a roof fall, since the closure rates in SPDV Room 1 accelerated almost vertically after this critical closure rate was reached. By using a curve fitting package, the best fitting equation for the closure rate of SPDV Room 1 was found. In order to simplify the fitting process and provide an accurate roof fall prediction, only the later closure measurements after 600 days were taken into account. The following form of equation was found to be the best for SPDV Room 1.

$$\dot{\varepsilon} = A + Bt^{C} \tag{3.2}$$

where, $\dot{\varepsilon}$ is the closure rate, t is the elapsed days since excavation, and A, B, and C are constants. The constants for SPDV Room 2 were determined and the collapse of SPDV Room 2 was predicted by extrapolating from the equation.

Since several uncertainties are involved when extrapolating a best fit curve, it is recommended that upper and lower prediction intervals be included. In this case, 90 % prediction intervals were used to determine the probable range of the roof collapse in SPDV Room 2. The prediction range was from February 1994 to February 1995 and the mostly probable date of Room 2 roof collapse was predicted as July 1994. This prediction turned out to be 1 month later than the actual roof fall which occurred in June 1994. The prediction curves for SPDV

Room 2 closure rate are shown in Figure 5.

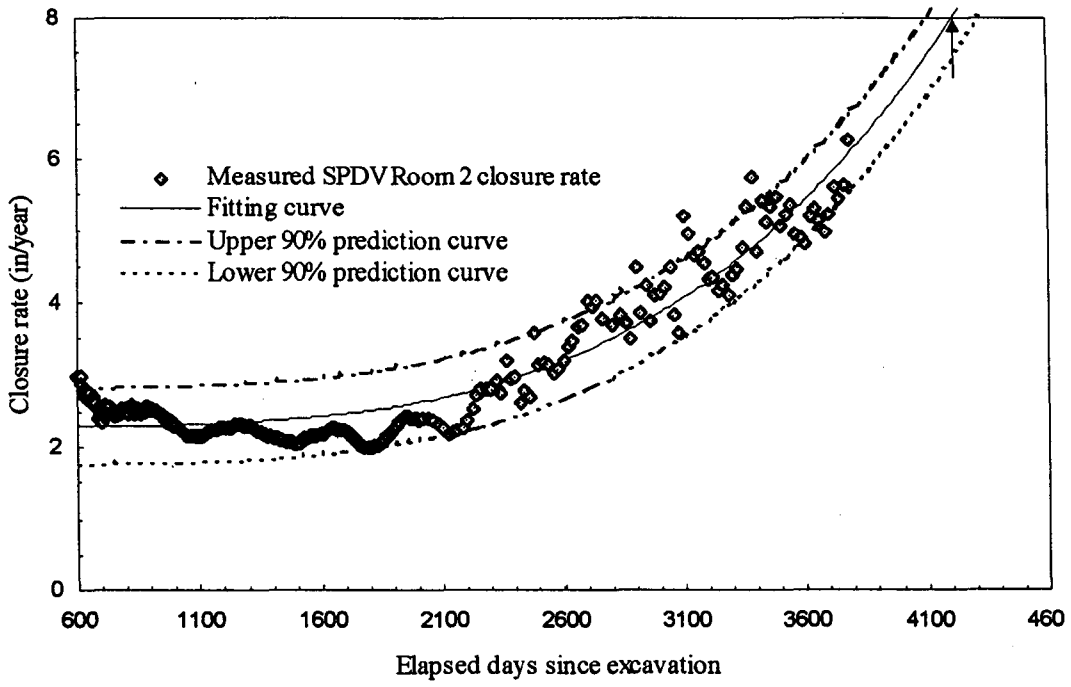

Figure 5. Prediction of the roof collapse in SPDV Room 2.

4. Calculation of the Zero strain boundary

Since the rock salt around underground excavations exhibits time-dependent deformation, the stress relief zone created by the excavation will change with time. The manner in which the boundary of the affected zone moves out from the opening is important in understanding the reaction of the rock to the stress change created by the excavation.

The extent of stress relief creep is particularly important for pillar design, since horizontal creep relief in pillars means a redistribution of overburden support, in addition to that lost by the excavation process. Using numerical analysis, it may be possible to calculate the boundary of the zone affected and thus the edge of the unaffected zone, called the "Zero Strain Boundary (ZSB)". The values obtained from such a numerical analysis, however, must be used with caution when applied to the design of underground openings and support systems, because of the inherent limitations of numerical methods.

Locating the unaffected boundary from field measurements is therefore potentially more useful as a method for understanding the deformational behavior of the rock strata around an opening. Unfortunately, no practical measuring technique exists for locating the boundary directly and curve fitting and extrapolation are not adequate for determining the boundary because extrapolation is strongly dependent on the choice of the curve. Furthermore, the best fit curve over the measured data points does not necessarily mean the best extrapolation curve. In this study, an indirect calculation technique for determining the location of the unaffected boundary was developed by using the relationship between the total extension and the convergence of an excavation. This technique was then applied to several locations at the WIPP site.

4.1 Calculation method

The total extension in the rock strata around an excavation, given by the summation of measured extensions in the ribs or roof and floor, should always be less than the corresponding total convergence. This is because the extension represents the displacement occurring only over the instrumented range, while the convergence represents the total displacement including that in the zone beyond the instrumented range. The method developed in this section calculates the location of the ZSB, and its migration rate from the difference between the total extension and convergence. The location of the ZSB was calculated using the following procedure after correcting and smoothing the data.

a. Calculate the extension between the surface of the opening and the end anchor.

b. Calculate the total extension from the sum of the roof and floor extensions or the sum of the extensions in the ribs.

c. Find the difference between the convergence and the total extension.

d. Plot the bay strain distribution with respect to distance from the excavation.

e. Calculate the location of the zero strain boundary, X , using the equations that follow. The area of the triangle in Figure 6, δ, is given by the equation:

$$\delta = \frac{1}{2}(X_0 - d_5)\varepsilon_2 \tag{4.1}$$

where, X0 is the location of the ZSB, d5 is distance from the opening, and ε2 is strain at the end anchor. δ should be the same as the difference between the total extension and convergence. Using the assumption of linearly decreasing bay strain from the last measuring point to the boundary, it is possible to derive the equation.

$$\varepsilon_2 = \frac{(X_0 - d_5)\varepsilon_1}{\left\{X_0 - \frac{(d_4 + d_5)}{2}\right\}} \tag{4.2}$$

where, d4 is the distance of the next inward station from the opening, and ε1 is the measured strain. From Equation (4.2) and (4.3),

$$\varepsilon_1 X_0^{\,2} - (2\varepsilon_1 d_5 + 2\delta)X_0 + d_5^{\,2}\varepsilon_1 + (d_4 + d_5)\delta = 0 \tag{4.3}$$

The location of the ZSB, X0, can be determined from Equation (4.4).

$$X_0 = \frac{2d_5\varepsilon_1 + 2\delta + \sqrt{(2d_5\varepsilon_1 + 2\delta)^2 - 4\varepsilon_1\left\{d_5^{\,2}\varepsilon_1 + (d_4 + d_5)\delta\right\}}}{2\varepsilon_1} \tag{4.4}$$

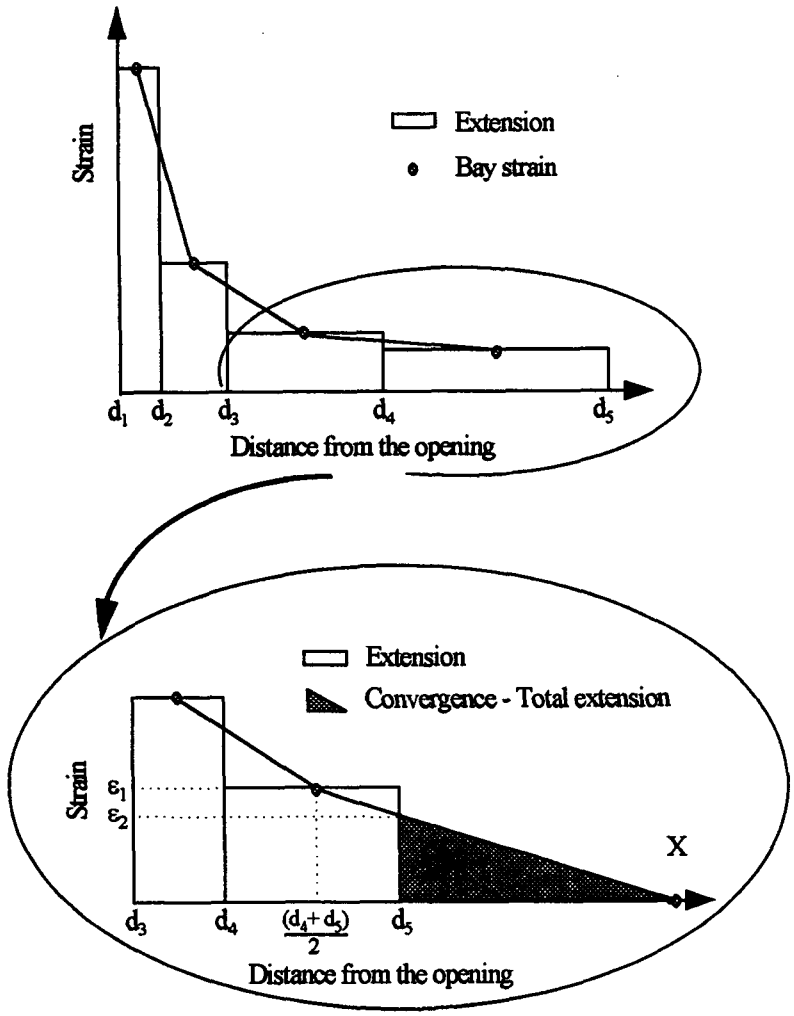

Figure 6. Determination of the ZSB from the strain-distance relationship.

Since d4 and d5 are known, ε1 and ε2 can be measured, and δ can be calculated from the total extension and closure measurements, it is possible to calculate the ZSB from the equation. The expansion rate of the boundary can be easily calculated once the location of the boundary has been identified at given time intervals.

Since the rock mass in a pillar is relatively homogeneous and the extension in each rib wall can be assumed to be equal, the above method can be directly used to calculate the ZSB in a pillar. In order to calculate the boundary in the roof and floor, the vertical convergence must first be separated into roof sag and floor heave.

4.2 Zero Strain Boundary in the abutment.

Based on the listed requirements, SPDV Room 1 East rib was selected to calculate the ZSB in mine pillar. The four rooms in the SPDV area were excavated in 1983. Many instruments, including extensometers, closure meters, and inclinometers were installed to investigate the deformation around the excavations. Six extensometers were installed in SPDV Rooms 1 and 2, three in the roof, one in the floor, and two

in the East and West ribs. The extensometers measured the displacements occurring in the first 15 m of the rock. Two convergence stations recorded horizontal and vertical convergences. Figure 7 shows the installation of extensometers and closure points in SPDV Rooms 1 and 2.

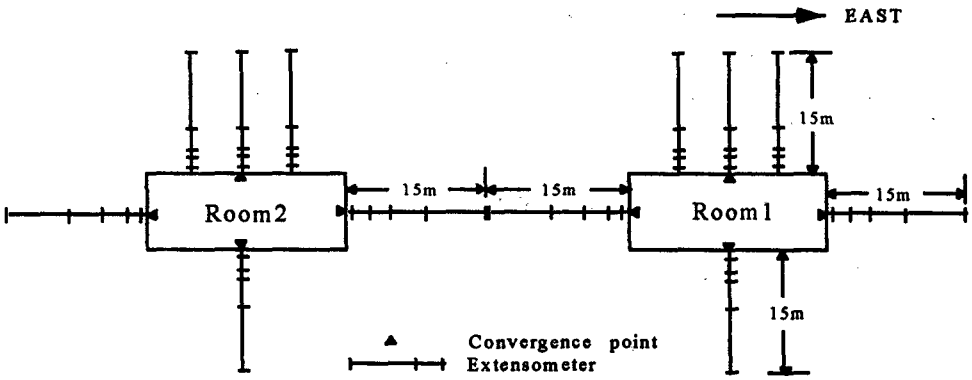

Figure 7. Instruments in SPDV Rooms 1 and 2.

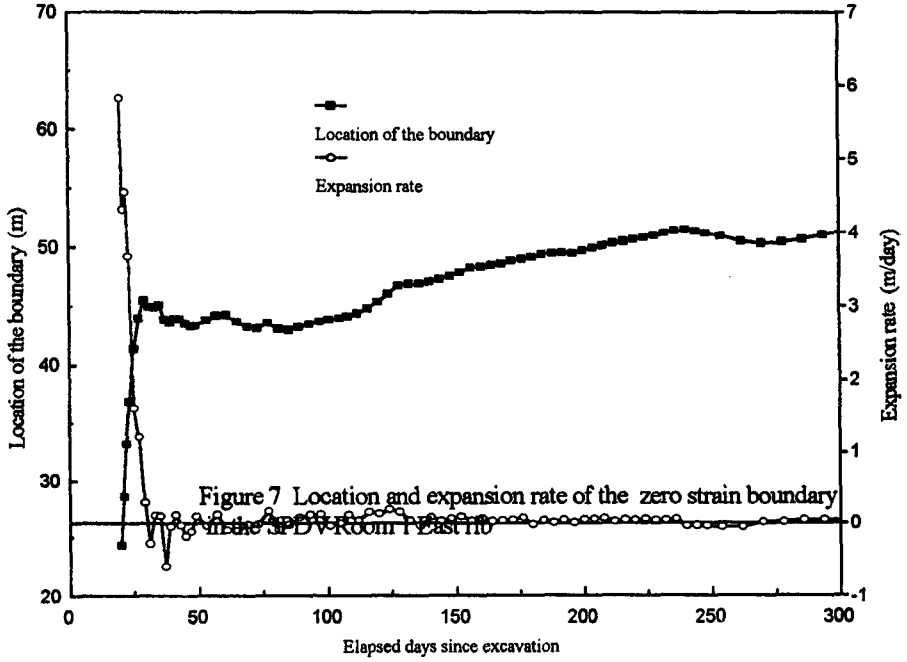

Figure 8. Migration of the Zero Strain Boundary in the SPDV Room 1 East rib

When SPDV Room 1 was excavated in April 1983, SPDV Rooms 2 and 3 had already been excavated. SPDV Room 1 East rib can be considered as a solid abutment because the distance to the neighboring excavation, the E0 drift , was about 70 m. Using the method described in the previous section, the location and migration rate of the ZSB were calculated and plotted in Figure 8. The migration rate of the boundary was high in the early stages after excavation, then decreased rapidly to near zero after 30 days. In other words, the size of the zone affected by the excavation of SPDV Room 1 increased rapidly in the first 30 days after excavation growing to a distance of 45 m from the opening.

5. A Proposed New Method for describing the Deformation OF AN EXCAVATION

Computer simulations are currently the most popular method to describe the deformational behavior of a rock mass around an excavation,. Even though these techniques have many advantages, there are clear limitations to their use. Firstly, if the in situ physical and mechanical properties of the rock are not precisely known, computer simulations cannot produce reliable results (Sakurai, 1991, 1993). Secondly, changes in the mechanical and physical properties of the rocks after excavation, are sufficiently significant that the values obtained from laboratory tests and used in the model cannot accurately predict the actual deformational behavior. Furthermore, the constitutive equations required to describe these property changes, which are dependent on time and distance from the opening, are extremely complex.

When a computer simulation does not have the capability of modeling the fracture mechanism around an excavation in salt and potash mines, the prediction from the simulation cannot accurately predict the deformational behavior of the opening. Thus the description of deformational behavior derived from a computer simulation can only be considered as a reference. When an accurate description of the actual behavior of an underground opening is required, it is desirable, if possible, to use actual deformation measurements instead of computer simulation. In this study, therefore, a new technique was developed to describe the actual deformation around an opening based on deformation measurements such as extension, closure, and inclinometer data. A FORTRAN program based on this new technique, calculates X and Y displacements at any location around an opening by using interpolation functions from the measured displacements.

5.1 Interpolation functions

Interpolation functions are widely used in computer simulation programs such as the finite element method. In Figure 9, displacements at any point between x1 and x2 can be determined from a single dimensional interpolation function, provided that the displacements d1 and d2 are given and the distance between point x1 and x2 is H.

$$d_y = \sum_{i=1}^{2} \varphi_i d_i \qquad (5.1)$$

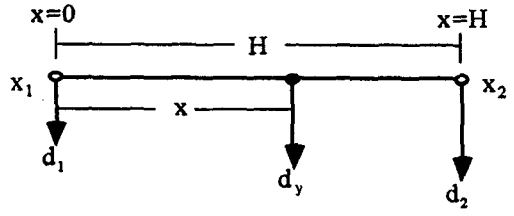

Figure 9. One-dimensional interpolation.

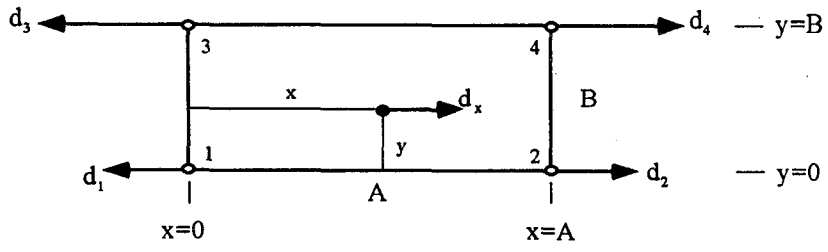

Figure 10. Two-dimensional interpolation.

where, the interpolation functions are

$$\varphi_1 = (1-\frac{x}{H}) \quad , \qquad \varphi_2 = (\frac{x}{H})$$

In Figure 10, if displacements d1, d2, d3, and d4 and the width and height of the element, A and B are given, then the displacement at a point, dx, can be calculated using the two-dimensional interpolation functions.

$$d_x = \sum_{i=1}^{4} \varphi_i d_i \qquad (5.2)$$

where,

$$\varphi_1 = (1-\frac{x}{A})(1-\frac{y}{B}) \quad , \qquad \varphi_2 = (\frac{x}{A})(1-\frac{y}{B}) \quad ,$$

$$\varphi_3 = (1-\frac{x}{A})(\frac{y}{B}) \quad , \qquad \varphi_4 = (\frac{x}{A})(\frac{y}{B})$$

5.2 Instrumentation

The program described is based on measurements from extensometers in the roof, floor, and ribs; closure meters; and inclinometers. Field data from SPDV Room 2 was used to describe the general deformation behavior of the rock mass around this opening at WIPP. In the SPDV Rooms at WIPP, a large quantity of deformation data was obtained, over a period of more than 10 years, from all the above mentioned types of instruments. Instruments installed in SPDV Room 2 and the measuring zones covered by each instrument, are given in Figure 11.

5.3 Calculation of displacements

a. Calculation of roof displacement. Three extensometers and two inclinometers were installed in the roof. The X displacement of any location can be calculated with the two inclinometers which were installed in the east and west sides of the roof. The Y

displacements can be determined from the three extensometers in the roof center, roof west and roof east. Figure 12 illustrates how to calculate the displacements in the roof. There are six measuring points, one convergence meter and five extensometers. From the measured extension, bay extensions Ecol-A, EA-B, EB-C, and EC-D can be determined by simple subtraction. The Y displacement of anchor D8 should be found first, from a comparison between roof convergence and total roof extension. In order to calculate D4 and D5 in Figure 12, the separation of the clay seam was calculated. Displacements at the other locations can be calculated in the same way.

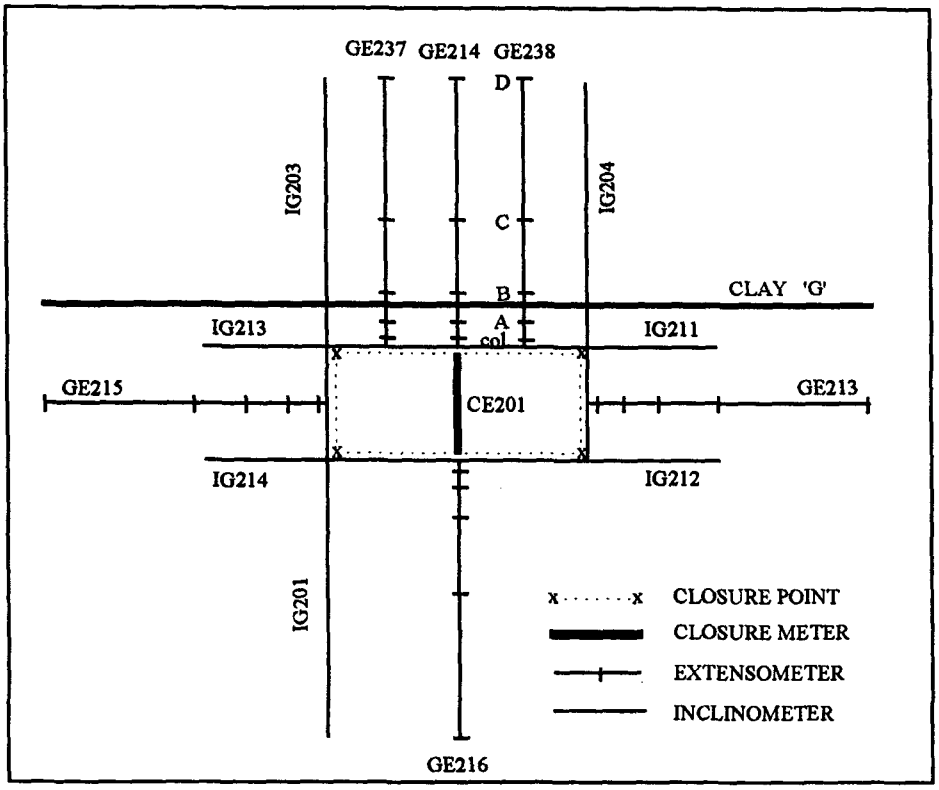

Figure 11. Instrumentation in SPDV Room 2.

b. Calculation of displacements at the corners. The location of each grid point should be defined before interpolation, since different instruments are used to calculate the X and Y displacements. The complete area was divided into four sections, roof, floor, East and West ribs. To find the boundary of each section, the angles $\theta 1$, $\theta 2$, $\theta 3$, and $\theta 4$ in Figure 13 were calculated from the X and Y displacement vectors at the four corners. The displacements at the corners can be derived from convergence data in the roof, floor, and ribs. The X displacements of the roof East and West corners were considered as being of the same magnitude but with opposite direction. Since the ratios of the displacement vectors in the corner points were not constant, the angles also varied with time. The separation at the clay seam in the four corners could be expected to be less significant so that the displacement distribution of the four corners was calculated from the displacement distribution of the rib. In the roof West corner, *Pxi* and *Pyi* were the calculated displacements at location (*xi*, *yi*).

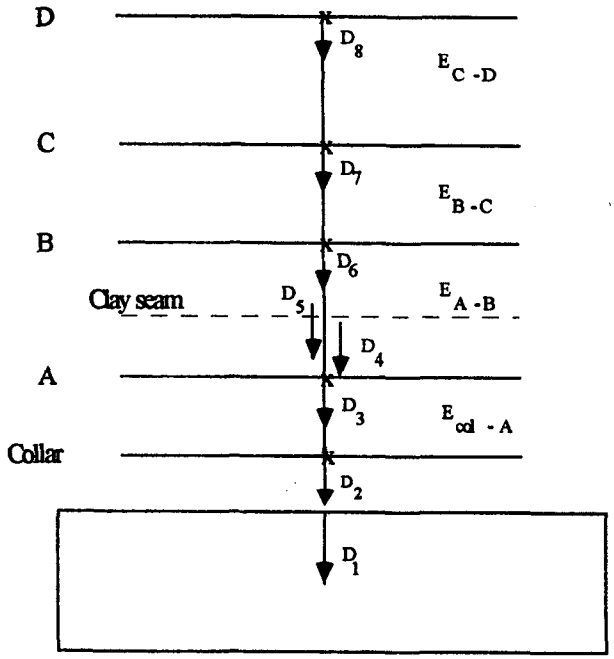

Figure 12. Calculation of roof displacements.

c. Calculation of X and Y displacements. In this program one or two-dimensional interpolation functions or a combination of them was used to calculate the displacements at any location. Figure 14 shows the four cases anticipated to occur in any calculation.

- CASE 1 : d1, d2, x, y and H1, H2 are needed to calculate the displacement, dx. To derive the displacement, a one-dimensional interpolation function was used twice.

$$d_x = \left\{(1-\frac{y}{H_1})d_1 + (\frac{y}{H_1})d_2\right\}(1-\frac{x}{H_2}) + (\frac{x}{H_2})d_3 \quad (5.3)$$

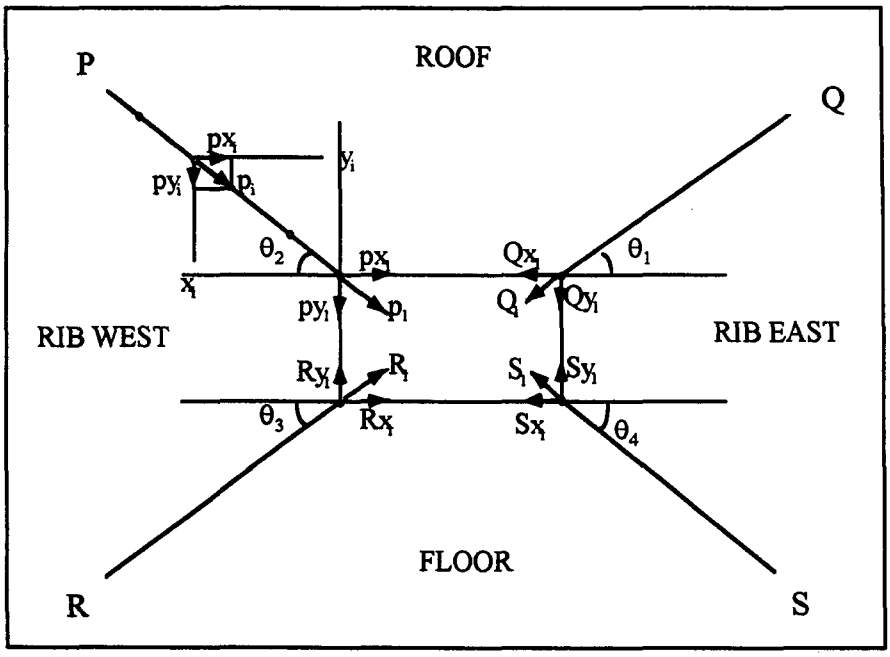

Figure 13. Displacements in the four corners.

- CASE 2 : A one-dimensional interpolation function can be used directly

(5.4)

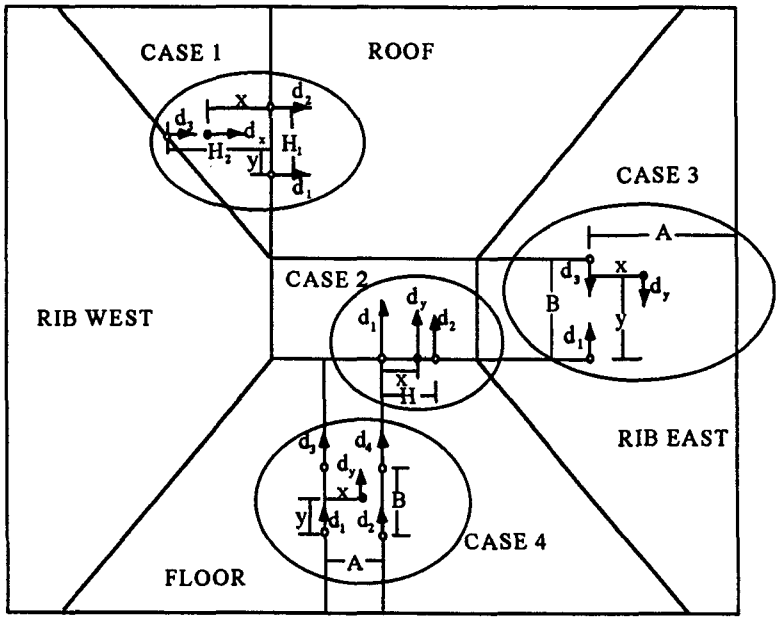

Figure 14. Four different cases.

- CASE 3 : The location of the zero vertical displacement boundary is assumed to obtain the displacements beyond the end point of the inclinometers which

were installed horizontally in the pillars to determine the vertical displacement of the pillars. The vertical displacement seems to decrease rapidly from the opening surface as shown in the deflection plots. In this case, it was assumed that there is no vertical displacement 50 feet from the opening, at the center of the pillar. From the two-dimensional interpolation functions with d2 = d4 = 0.

$$d_y = (1-\frac{x}{A})(1-\frac{y}{B})d_1 + (\frac{x}{A})(1-\frac{y}{B})d_3 \quad (5.5)$$

- CASE 4 : Two-dimensional interpolation functions must be used.

$$d_y = (1-\frac{x}{A})(1-\frac{y}{B})d_1 + (\frac{x}{A})(1-\frac{y}{B})d_2 + (1-\frac{x}{A})(\frac{y}{B})d_3 + (\frac{x}{A})(\frac{y}{B})d_4 \quad (5.6)$$

5.4 Calculation of opening area

After the excavation, the opening area decreases due to the time-dependent deformation of the rock around the opening. The change in area of the room was calculated by using a program routine written in FORTRAN.

Based on the calculated X and Y displacements derived from the program, several figures plotting grid changes, resultant displacements, and accumulated volumetric strains, could be obtained from the FLAC routines. Figure 15 shows the opening area change at different times. The opening area decreased rapidly immediately after excavation and then decreased at a constant rate. Figure 16 shows the opening deformation 6 years after excavation.

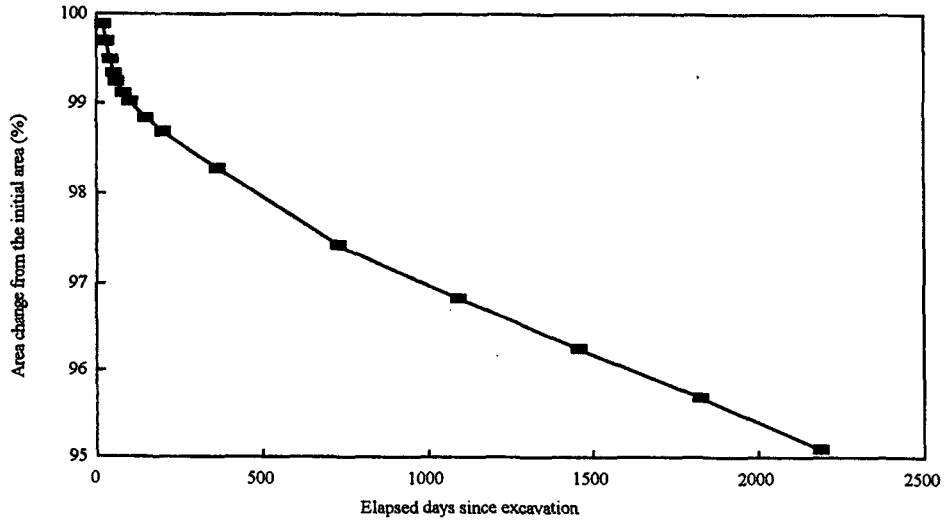

Figure 15. Predicted opening area change with time.

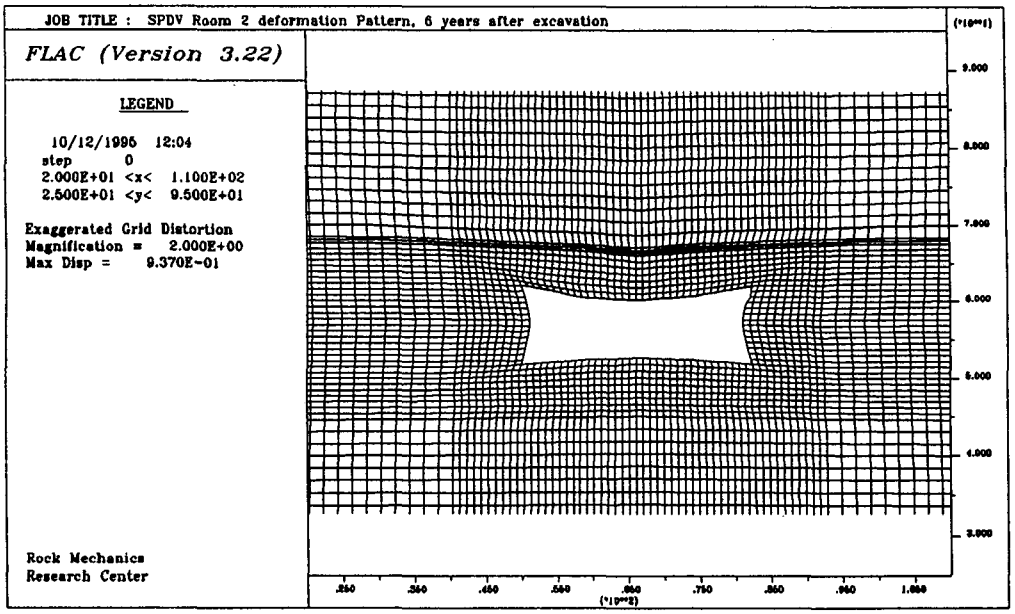

Figure 16. Actual deformation of SPDV Room 1 in 6 years after excavation.

6. Deformation prediction of underground excavations at WIPP using Backpropagation

The information derived from actual measurements can be applied directly to other in situ conditions, while computer simulations and laboratory tests need many assumptions for applying the results to mining design. This is a great advantage of utilizing in situ measurements for understanding the actual deformation mechanism and predicting the deformational behavior of underground excavations. Regression analysis techniques are applicable in many cases to derive the relationships between input and output. However, they become progressively more difficult to predict output using regression analysis, as the number of parameters increases. Since there are a large number of parameters, regression analysis may not be adequate. The application of Neural Networks (NN) can be a more powerful alternative for predicting the deformational behavior of an opening and for deriving the relationships between deformation and each parameter, for the following reasons. Firstly, NN can use qualitative information such as rock type, bed type, or excavation method as input or output. Secondly, there is no limit to the number of inputs or outputs. Thirdly, NN can be used to solve complicated nonlinear problems, and complex relationships between input and output. Finally, NN is capable of modeling input-output functional relations, even when mathematically explicit formulas are unavailable (Szewczyk and Hajela, 1994).

6.1 Introduction to Neural Networks

The human brain is a very complex biological network of hundreds of billions of special cells called neurons and connections between neurons, called dendrites. Figure 17 shows the major components of a typical biological nerve cell. Each neuron is connected to 1,000 or more other neurons through its branching mesh. These neurons

transmit an electrical impulse received from neighboring neurons through a channel, called an axon, to other connected neurons. When the pulse reaches the end of the axon, it must cross a gap about a millionth of an inch wide, called a synapse, in order to reach the neighboring neurons. When the electrical signal stimulates the axon, a chemical substance referred to as a "neurotransmitter" will be released. The neurotransmitter moves to the dendrites of the receiving neuron and generates an electrical impulse. Depending on the chemical substance generated, different electrical signals can be formed in the synapse; either excitatory or inhibitory. The different electrical input signals from the numerous neighboring neurons are summed at the axon hillock. When the amount of depolarization stored at the axon hillock is sufficient, an action potential is generated and travels down the axon away from the main cell body. In this manner, a conversion occurs between a electrical signal and a chemical signal, and a message can be continuously transmitted from one neuron to another until the impulse no longer exceeds the threshold at the axon hillock. There are a few theories about how the brain can learn, but the general opinion is that learning in the brain occurs in the form of changes in the synapses when signals are received (Lawrence, 1993).

Artificial Neural Networks are formed of simulated neurons, connected in a similar way to the neurons in a human brain and thus are able to learn in a similar manner as the human brain, as shown in Figure 18.

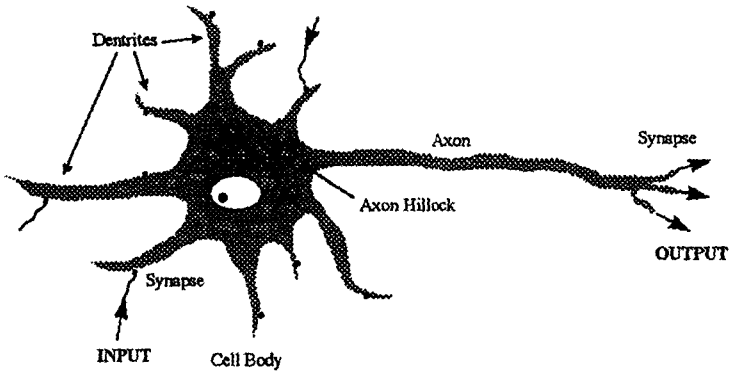

Figure 17. Typical biological neuron.

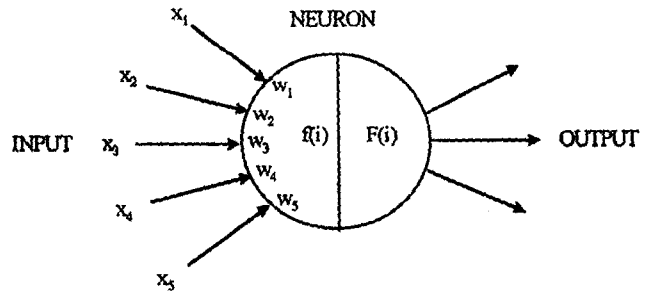

f(i) = w1x1 + w2x2 + w3x3 + w4x4 + w5x5 , F(i) = Transformation of f(i)

Figure 18. Artificial neuron.

The basic process in Neural Networks can be divided into four steps; (a) input to the neurons; (b) summation of the net values calculated by multiplying the weight values and input values of the individual input signals; (c) transformation of the net value; and (d) output to the next neuron. Input in Neural Networks simulates the electrical signal coming from the synapses. Calculation of the net value simulates the summation of

the potential delivered from the neighboring neurons at the axon hillock. The weights in Neural Networks serve a similar function to the neurotransmitter in the synapse, because it is the weight in the Neural Network which determines whether the input signal is excitatory or inhibitory. Transformation of the net value is required to simulate the function of the axon hillock which determines whether the signal can be transmitted to the next neuron or not. Similar to the human brain, Neural Networks are highly parallel dynamic systems that transfer information by means of their overall state response to input. Sometimes this is called an artificial neural system, neural intelligence, or neurocomputer. After the initial Neural Network model was developed in 1943, many other techniques including Backpropagation (BP) were developed. Each technique has it's own characteristics and can be applied to different areas, mainly for noise reduction, pattern recognition, performance prediction, and performance optimization.

6.2 Backpropagation

Backpropagation (BP) is a multi-layer feed-forward network that uses a supervised learning method in which an error signal is fed back through the network and changes network values to correct the error and to prevent the same error from happening again (Lawrence, 1993). It is the most commonly used Neural Network model because it provides a mathematical explanation for the dynamics of learning and has proved to be consistent and reliable when applied (Lawrence, 1993). BP is suitable for predicting opening deformations, since most of the input and output values are analog. Many of other Neural Network models which require binary or bipolar information, are not suitable for predicting the relationship between analog input and output.

a. Structure of the Backpropagation network. In BP, three-layer and four-layer networks are most popular. The three-layer network consists of three layers, input, hidden, and output layers. The three-layer BP architecture is shown in Figure 19. The input layer neurons send information to the hidden layer neurons between the input and output layers. The number of neurons in each layer depends on the number of input and output parameters. There is no formula to determine how many hidden neurons are best for the network, because it seems to be largely dependent upon the complexity of the problem being solved (Lawrence, 1993). One rule of thumb is to use the average of the number of inputs and the number of output neurons (Lawrence, 1993).

Each connection has a weight which can represent the strength of the relationship between connected nodes. During network training, the weights of the connections are changed to minimize the overall error term. The error of the network is determined by comparing the desired output and calculated output. In Neural Networks, changing the weights is called learning. Bias terms can be included to help to obtain convergence of the weights to an acceptable solution (Freeman and Skapura, 1992).

b. Activation function. The activation function is applied to the net input of a neuron and determines the output from the neuron. Its domain must be all real numbers, as there is no theoretical limit to the net input (Master, 1993). The range of the activation function is usually limited and usually range between 0 and 1, but some range from -1 to 1. Early neural models used a simple threshold function as following:

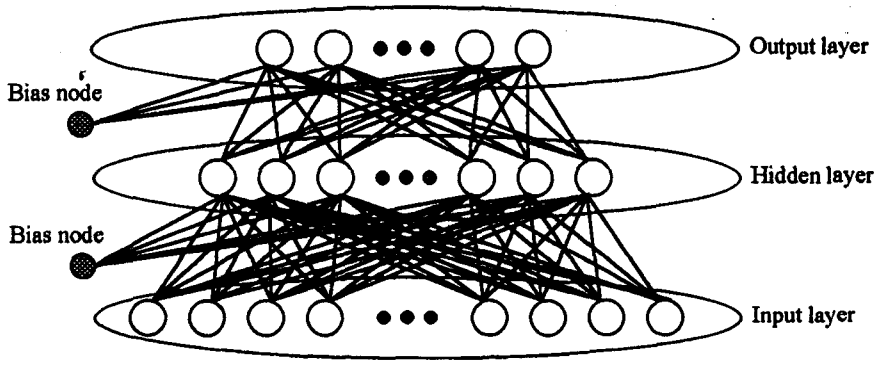

Figure 19. Architecture of three-layer Backpropagation.

$$f(x) = \begin{cases} 1, x \geq \delta \\ 0, x < \delta \end{cases} \tag{6.1}$$

where, δ is the threshold value. If the weighted sum of inputs is less than the threshold, the neuron's output is 0, otherwise the output is 1. In some models the output would be the weighted sum itself, if the threshold value were exceeded (Master, 1993).

There are great advantages to the activation function, being differentiable in describing the learning mechanism of the network mathematically. Since the threshold function is not differentiable, many Neural Network models, including BP, use a sigmoid activation function, which is differentiable but otherwise acts in a similar way to the threshold function. Figure 20 shows the characteristic S-shape of the sigmoid function and typical threshold function. The typical sigmoid function is

$$f(x) = \frac{1}{1+e^{-x}} \tag{6.2}$$

A sigmoid function is a non-linear but continuous, real-valued function whose domain is real, whose derivative is always positive, and whose range is bounded. In most cases, it has been found that the exact shape of the function has little effect on the ultimate power of the network, though it can have a significant impact on the training speed.

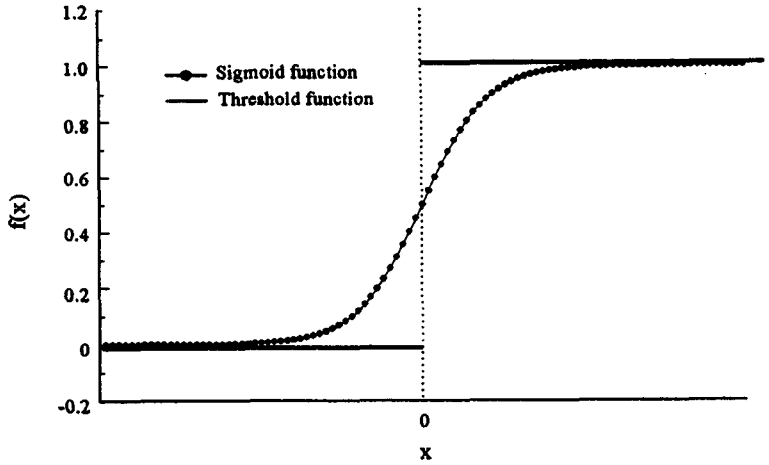

Figure 20. Typical activation functions.

c. Generalized delta rule. BP network uses a generalized delta rule as the learning algorithm. The learning rule is the most important part of a Neural Network, since it determines how the weights are adjusted as the Neural Network gains experience (Lawrence, 1993). For a single output unit k, the error is the difference between the desired output value Yk and the calculated output Ok .

$$\Delta_k = Y_k - O_k \tag{6.3}$$

During a program run, the sum of the squares of the errors for all output units should be minimized.

$$E = \frac{1}{2}\sum_{k=1}^{m} \Delta_k{}^2 \tag{6.4}$$

With the generalized delta rule, the network can reduce the sum of the squared error at each iteration step, by changing the weights applied to all the connections.

6.3 Deformation prediction using backpropagation

Extensive investigations have been carried out in order to understand the deformation mechanism of underground excavations in salt using laboratory tests, in situ measurements, and computer simulations. However, any of this previous work could not accurately predict the deformational behavior of a newly implemented opening design, because of the complexity of the time-dependent properties of rock salt. Prediction by a NN trained by field measurements will be more accurate than a computer simulation, since the field measurements incorporate all factors related to the complex property change.

a. Backpropagation structure. To predict the deformation of an underground excavation, the important parameters must be identified. Based on the previous

data analyses, the following 12 parameters were chosen as the input for the network: (a) depth of opening; (b) elapsed time after excavation; (c) installation date of instrument; (d) opening width and height; (e) maximum and minimum pillar sizes; (f) location of the measuring point; (g) thickness of the immediate roof layer; (h) excavation method; (i) deposit type; and (j) rock type. A three-layer BP network was used to predict the deformation of the underground openings at WIPP. The three layers consist of 12 input nodes, 5 hidden nodes, and 1 output node. Bias terms for the hidden and output layers were included to increase the calculation speed.

b. Data collection and training. A measured deformation curve can be divided into two stages, the primary creep stage and the secondary creep stage. In the primary creep stage, the opening deforms rapidly and the amount of deformation is very sensitive to the surrounding conditions, while it deforms at an almost constant rate in the secondary creep stage. If the opening deformation in the primary stage can be predicted precisely, prediction of the secondary creep stage is relatively easy. Thus, closure data collected for the first 200 days after excavation were used to predict the primary deformation. The period of 200 days is selected as the transition time from the primary to secondary creep stage based on the previous data analyses. In order to train the network, 178 data points were chosen from 26 closure points. The selected inputs and output were normalized and used to train the BP network. The learning rate of 0.2 was used for training the data. Figure 21 shows a comparison between the measured and calculated closures after training.

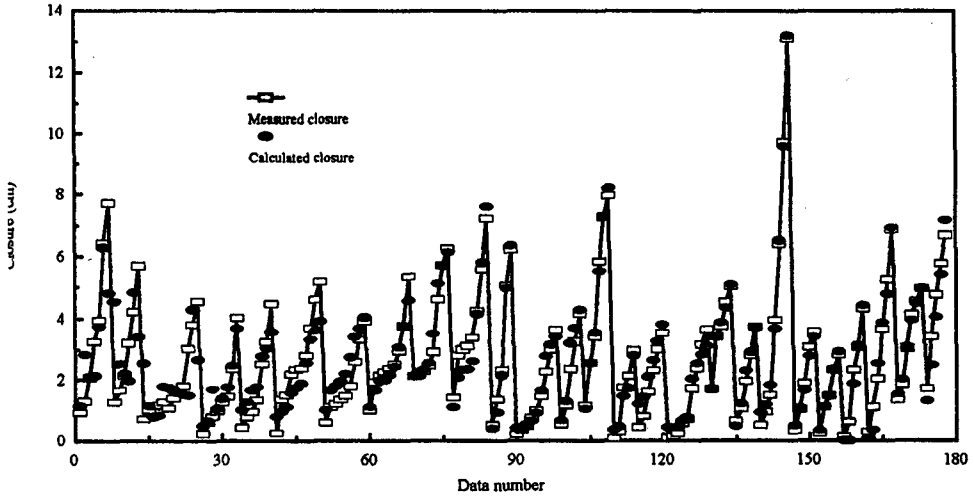

Figure 21. Comparison of predicted and measured closure.

c. Influence of installation date. The measured closure is not the total deformation of an excavation since it was excavated, but that of the excavation since installation of the instrument. Figure 22 illustrates the influence of the installation date on the vertical closure. In Figure 22, each curve represents vertical closure at a specific time after excavation. The bottom curve is the predicted closure 10 days after installation. The closures vary with respect to the elapsed time following installation. From these curves, the initial closure which could not be measured because of late installation, can be estimated. In the case

of the curve for 50 days, if the instrument was installed 10 days after excavation, the closure deformation from the excavation until installation of the instrument was about 6.6 cm. This means there would be 6.6 cm difference in the total closure at 50 days after excavation between the two measurements at the same position with different installation dates: one is installed immediately after excavation and the other is installed 10 days after excavation. The influence of the installation date is much more significant in the early stages compared to the later stage. Thus, it is advisable to use deformation rates instead of deformations, when comparing two sets of data.

d. Influence of opening width. Figure 23 shows the increased closure with respect to time for the opening widths; 3 m, 4.8 m, and 6.6 m. Vertical closure increases as the opening width increases, but the effect of width increase is not the same for different opening sizes. The influence due to 1.8 m increase in the opening width from 3 m to 4.8 m is less than the increase as the width grows from 4.8 m to 6.6 m. The significant increase in the deformation rate with opening size in the later stages indicates that this effect prevails for a long time. Thus, it could be concluded that the opening size is an important factor in determining the overall deformation in an excavation in rock salt.

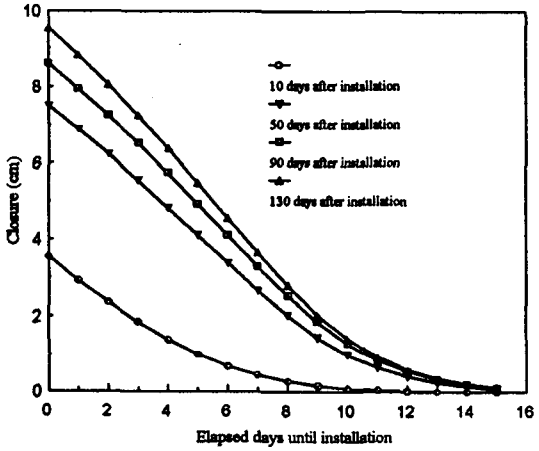

Figure 22. Influence of installation date.

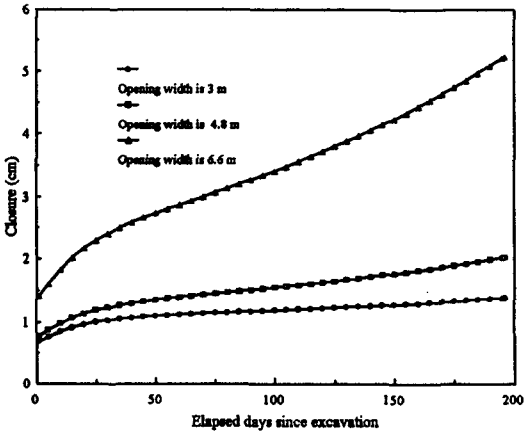

Figure 23. Influence of opening width.

e. Influence of pillar size. Figure 24 shows the effect of the pillar size (width) on the closure rate. All curves in Figure 24 show a similar pattern of an exponentially decaying curve. As the pillar size increases, the opening closure rate decreases. The influence of the pillar size is more significant in the early stages. About 100 days after excavation, the differences in the closure rate become negligible. This shows that the pillar size is more important during the early stages.

f. Influence of measuring location. At WIPP, as in most salt mines, roof conditions at intersections are generally better than in locations remote from intersections (U.S.DOE, 1993). In an underground intersection, the salt mass is less confined and has more freedom to creep towards the opening, since the corners of the pillars around the intersection tend to yield easily. This leads to a lower concentration of shear stress in the roof and as a result the roof is more stable. In Figure 25, the

trained network predicts a higher deformation rate in the early stages at four-way intersection than two-way and three-way intersections.

g. Prediction of vertical closure. The trained network was applied to predict the vertical closure at a measuring point, which was not included in training. Figure 26 shows the prediction of vertical closure compared to the measurement. The difference between these measurements and the predictions is due to other parameters such as temperature, adjacent excavation, underground water, and support, which could not be included during training because of insufficient information.

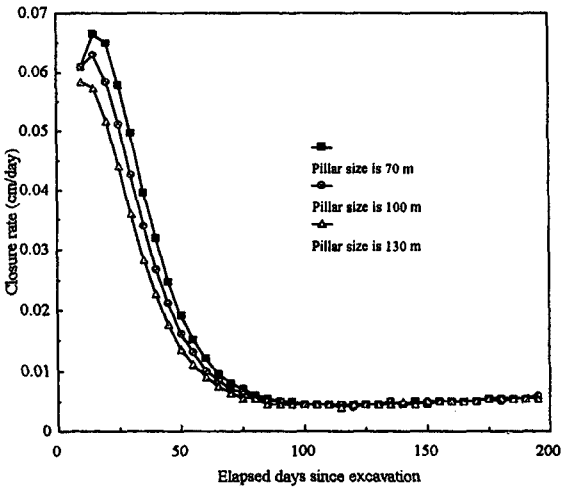

Figure 24. Influence of pillar size.

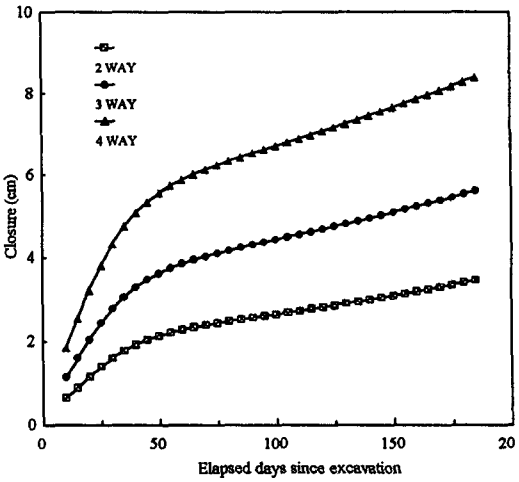

Figure 25.Influence of measuring location.

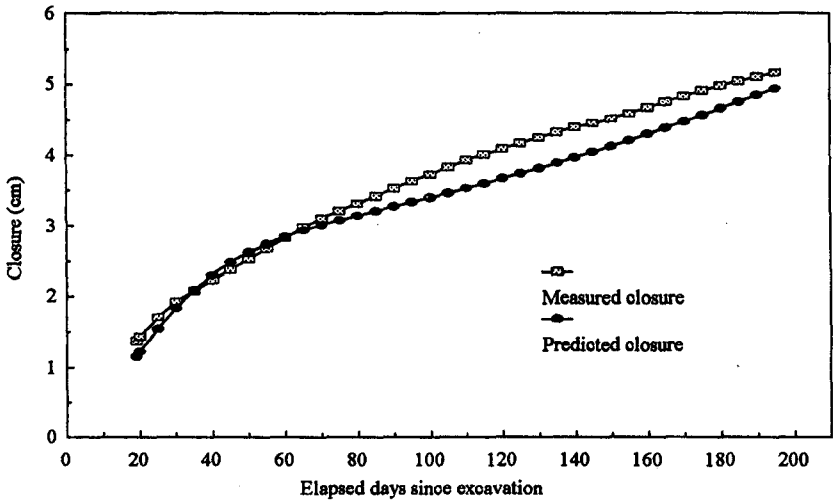

Figure 26. Prediction of vertical closure at a measuring point.

7. CONCLUSIONS

In this study, extensive data analyses from the in situ deformation measurements made at the WIPP and other salt and potash mines have been carried out in order to understand the deformation mechanisms around underground excavations in salt and

potash mines. The measured deformations were compared with the results of computer simulations of different cases to determine the limitations as well as the possibilities for computer simulation of salt and potash mine operations. In order to use the in situ measurements for specific purposes, such as the calculation of bed separation, the determination of the ZSB, or to provide a description of the stress and strain distribution around an excavation, several new techniques were developed. Finally, a Neural Network was used to compensate for the limitations of the computer simulation and statistical methods in developing a better prediction of the deformational behavior in salt and potash mines. From these studies, conclusions related to the overall deformational behavior of underground excavations as well as to the opening stability, have been drawn. Furthermore, several suggestions have been developed for a better understanding of the deformation mechanism in and around openings in salt and potash mines.

7.1 New techniques developed in this study

In this study, several new techniques were developed to enhance the value of in situ measurements in providing a better understanding of the deformational behavior of underground excavations:

a. A technique for determining the optimum measuring interval was suggested. In order to achieve reliable deformation rate curves, frequent acquisition is required, however, this must be offset by cost considerations. Thus it is necessary to measure deformation at an optimum time interval. The technique suggested in this dissertation determines the measuring interval based on the deformation rate and as a function of instrument noise. By following this technique, the percentage of instrument noise in the deformation change during the measuring interval is maintained as a constant.

b. A new term "Zero strain boundary (ZSB)" was established and defined. This boundary of the zone affected by the excavation, was calculated using a newly developed equation and the relationship between closure and total extension. The results of the calculation were used to describe the general pattern of shear stress distribution around an excavation.

c. Excavation deformation was described using field measurements. A new technique was developed to display the actual deformation change which occurs around an opening with respect to time, using field measurements. In this technique, a two-dimensional interpolation function was used to calculate X and Y displacements at the grid points.

d. Neural Networks were applied and shown to be a valid method for use in predicting the opening deformation and a tool to understand the overall deformational behavior of the excavations.

7.2 Investigations of deformation mechanism

a. From the measurements at WIPP and other mines the transition times from the primary creep to the secondary creep states were determined from the Box-Whisker plot of the deformation rates and the plot of deformation acceleration. At WIPP, the transition time from the primary to the secondary creep stage occurred about 200 days after the excavation is made. After 200 days, the

deformation rates for different locations decreased to similar values.

b. From the wide distribution of deformation rates in the early stages of room existence, it was concluded that these rates were sensitive to controlling factors such as opening geometry, prevailing stress conditions, room temperature, etc.

c. Opening width is one of the most important parameters in determining the overall deformational behavior around an opening. The influence of opening width was observed even in the steady state creep stage. The secondary creep rates of the roof tend to increase with greater opening widths. Similar results were derived from a trained Neural Network model of an opening. The network showed that the deformation rate increased with an increase in opening width and this influence prevailed over a long time interval.

d. The measured deformations at the WIPP site showed the significant influence of seasonal temperature variations on deformation rates. The temperature effect on the deformation rate was investigated and the following equation for predicting the relationship was suggested from this study.

$$\dot{\varepsilon} = \left\{A + B\cos(\frac{2\pi}{360})\right\}\left\{e^{-\frac{Ct}{365}}\right\} + \left\{D + E\exp(-\frac{t}{F})\right\} \quad (7.1)$$

where A, B, C, D, E and F are constants and t is the number of elapsed days since excavation. The first part of the equation expresses the periodic variation and the second part represents the decay of the temperature effect with time. The last part is used to describe the general decay pattern of the deformation rates without the temperature effect.

e. The influence of mining adjacent excavations on an opening is an important parameter to be included in mine design, particularly when defining the mining sequence. In this study, data was insufficient to determine the effect of adjacent excavations on the stability of previously excavated openings, and to determine an adequate mining sequence.

f. The zone unaffected by an excavation, the ZSB, was calculated by comparing the total extension and the closure measurements. The location of the ZSB initially moved rapidly away from the opening in the early stages after its creation. For instance, the ZSB in SPDV Room 1 East rib migrates rapidly to a distance of 50 m from the opening during the first 30 days and then it moves very slowly after that time.

g. Using a descriptive process for the actual deformation of the rock around an opening, it was possible to calculate the opening area change with time. The opening area decreased rapidly in the early stages of deformation and then the rate steadily slowed to a constant value.

h. The influence of pillar size on the deformational behavior of an excavation was estimated using a Neural Network. From the trained network, it was found that the closure rate decreases with larger pillar sizes and that the influence of the pillar size is more significant on deformation in the early stages of the opening life.

i. The Neural Network predicted different deformational behaviors for the excavation depending on the layout at the measuring location. A higher deformation rate especially in the early stages, was predicted at four-way intersections in contrast to that at two-way and three-way intersections.

7.3 Suggestions for better understanding of the deformation mechanisms

The following suggestions are made to help in describing the deformation mechanisms of underground excavations in rock salt more accurately.

a. Use deformation rate. The instrumentation installation date following mining is important in establishing the amount of overall deformation of an excavation. When there is a time delay in installing instruments after mining, the large elastic and primary creep deformations which occurs immediately after excavation are often missed and the amount of deformation may be misjudged. It is therefore useful to use deformation rates, such as closure rate or rock extension rate, instead of cumulative deformation as a means of comparing data from different sites as well as for evaluating the results of computer simulations. Deformation rates are useful as a means of understanding the deformation mechanism of underground openings, for the following reasons: (a) deformation rates (when comparing two sites) are independent of the installation date of the instruments; (b) deformation rates can clearly show the influence of excavating a subsequent adjacent excavation; (c) influence of temperature can be clearly recognized; and (d) deformation rates are closely related to the stress distribution around the excavation.

b. Measure the deformation using an optimum measuring interval. The weakness of deformation rate terms is that they can be influenced by the choice of the measuring interval. The fluctuation frequently observed in the deformation rate curves does not necessarily represents a change in the deformation mechanism, but it is often related to an improper choice of the measuring interval. In order to determine more reliable deformation rates, deformations must be recorded at optimum measuring intervals, especially in the period immediately after excavation.

If the deformation rate and instrument noise in situ are known, the optimum interval can be determined easily. If not, they must be estimated indirectly in the following ways: (a) use the previously measured deformation rates to estimate the next measurement interval; and (b) estimate the in situ instrument noise by comparing the curves developed using a variety of measuring intervals.

c. Data smoothing and interpolation. Smoothing the data before calculating deformation rates is useful as a means of decreasing the fluctuations in numerical rates. Smoothing should be carried out with caution, because it can remove valuable information from the original data. For instance, when there is a sudden increase in displacement rate due to the creation of a neighboring excavation, smoothing can hide the size of this effect. Thus data smoothing should be carried out separately before and after the adjacent excavation is mined. A three-point moving average method was found to be adequate for treating field measurements from the WIPP site.

With the interpolation of the deformation measurements, it was possible to compare the deformational behavior from different measuring sites and over different measuring intervals.

d. Plot the strain vs. distance relationship. Plots of bay strain distributions with respect to the distance from an opening is a useful way for understanding the overall deformation mechanism around an opening. For example, the ZSB and the separation over a clay seam could be determined from the plot. More accurate evaluation of opening behavior, including the detection of fracture planes, may be possible with more measuring stations along a borehole and with a smaller distance between anchors.

e. Consider the influence of adjacent excavations. The deformation increase

after the creation of an adjacent excavation is the result of the reaction of the rock mass to the sudden stress change caused by the new adjacent excavation. Therefore, if this deformation is measured carefully, it can be helpful in understanding the deformational behavior of the rock salt immediately after excavation, which is related to sudden stress change and cannot be measured since the elastic deformation occurs before the installation of instruments.

f. The importance of the installation date of an instrument was clearly determined from the Neural Network trained using the in situ measurements at WIPP. It is, therefore, recommended that instruments should be installed as soon as possible and thus measure the primary creep deformation in order to monitor the complete deformational behavior of an underground excavation. Measurement of the early stages of deformation is important to investigate the influence of controlling parameters on the deformational behavior of an excavation, since this influence is more significant during the early deformation phase.

g. In order to calculate the ZSB more accurately, the length of the last bay should be short enough to satisfy the assumption of linear decreasing strain. It also should be kept in mind that too short a bay length can result in fluctuation of the measurements due to the influence of instrument noise. Thus, the location of the last anchor should be decided from the estimated location of the ZSB and the level of instrument noise.

h. In order to describe the actual deformational behavior of an excavation from in situ measurements, it is necessary to install a variety of different instruments around an opening, such as extensometers, closure meters, closure points, and inclinometers.

i. Compare measurements with simulation results. It is highly recommended that the results of any computer simulation should be validated before using them to draw conclusions. This validation should use field measurements to calibrate the assumptions used in the simulation model. The deformation increase due to the creation of an adjacent excavation is quite useful for this purpose. Since it is possible to measure the sudden deformation increase caused by an adjacent excavation in the field, using previously installed instruments, a direct comparison can be made between the computer simulation and field measurements. From such comparisons, the parameter values to be used in the constitutive equation for the mine rock, can be determined.

j. Use Neural Networks for data analysis. After training the Neural Network with measured closure measurements from the WIPP site, the network was used to predict the deformation of an excavation and to define the relationships between the deformation and the associated parameters such as time after excavation, installation date, location of measurement, opening width, and pillar size. In order to apply the Neural Networks to salt and potash mines and to predict the deformation more accurately, the following steps are recommended: (a) use the deformation rate instead of deformation to simplify the network by removing one input node for installation date; (b) in order to apply the network to salt and potash mines, panel width should be included; (c) to predict the deformation of an excavation completely, it is necessary to build a new network which can predict the influence of adjacent excavations; and (d) read all possible information about the measuring location.

References

Freeman, J.A. and Skapura, D.M. (1992): Neural networks. Addison-Wesley Pub. Co.,

Massachussetts.

Hansen, F.D., Mellegard, K.D., and Senseny, P.E. (1981): Elasticity and strength of ten natural rock salts. First conf. on the Mechanical Behavior of Salt, Pennsylvania State University, University park, 71-83.

Lawrence, J. (1993): Introduction to neural networks. California Scientific Software, Nevada City.

Master, T. (1993): Practical neural network recipes in C++. Academic Press, Inc., Santiago, CA.

Sakurai, S. (1993): Back analysis in rock engineering. Comprehensive Rock Eng. 4, 543-569.

Sakurai, S. (1991): Computational methods in rock mechanics. Proc. of the 7th International Cong. on Rock Mechanics, Aachen, Deutschland, 1563-1570.

Szewczyk, Z.P. and Hajela, P. (1994): Damage detection in structures based on feature-sensitive neural networks. J. of computing in civil engineering 8, 163-178.
U.S.DOE (1989): Geotechnical field data and analysis report, June 1987 - June 1988. DOE/WIPP 89-009.

U.S.DOE (1993): The current bases for roof fall prediction at WIPP and a preliminary prediction for SPDV Room 2. DOE/WIPP 93-033.

Verdeman, S.B. (1993): Statistics for engineering problem solving. PWS publishing Co., Boston.

Wittaker, B.N., Singh, R.N., and Sun, G. (1992): Rock fracture mechanics: Principles, design, and applications, New York.